Mixed Stochastic-Deterministic Approach for Many-Body Perturbation Theory Calculations

Aaron R. Altman, Sudipta Kundu, and Felipe H. da Jornada

Phys. Rev. Lett. **132**, 086401 — Published 20 February 2024

DOI: 10.1103/PhysRevLett.132.086401

Mixed Stochastic-Deterministic Approach for Many-Body Perturbation Theory Calculations

Aaron R. Altman,[1] Sudipta Kundu,[1] and Felipe H. da Jornada[1,2,†]

[1]*Department of Materials Science and Engineering, Stanford University, Stanford, CA 94305, USA*
[2]*Stanford Institute for Materials and Energy Sciences, SLAC National Accelerator Laboratory, Menlo Park, CA 94025, USA*

We present an approach for GW calculations of quasiparticle energies with *quasi-quadratic* scaling by approximating high-energy contributions to the Green's function in its Lehmann representation with effective stochastic vectors. The method is easy to implement *without altering the GW code*, converges rapidly with stochastic parameters, and treats systems of various dimensionality and screening response. Our calculations on a 5.75° twisted MoS_2 bilayer show how large-scale GW methods include geometry relaxations and electronic correlations on an equal basis in structurally nontrivial materials.

Many-body perturbation theory (MBPT) within the first-principles GW approximation is a proven and widespread method for computing accurate quasiparticle (QP) properties of materials [1–5]. Obtaining fully converged QP energies within the GW approach for small to moderately sized *bulk* systems, with up to a few hundred atoms in the unit cell, is a routine procedure with modern high-performance supercomputers [6–9]. However, exploring the more complex many-body physics of large systems that are relevant in electronic and technological applications is difficult due to the quartic scaling in system size of the standard GW formalism [2], limiting the applicability of the method in large-scale problems such those involving twisted materials displaying moiré physics [10–17].

Several approaches have been developed recently to deal with these shortcomings. They fall mainly into two categories: modifying the standard reciprocal-space GW formalism, wherein the electronic Green's function G is still evaluated in its Lehmann representation as a sum-over-bands, or employing different representations of the theory that avoid the explicit sum-over-bands. Notable techniques in the former category include replacing high-energy orbitals with simple ansatz wavefunctions and using completion relations to truncate the sum-over-bands [18–22]. Approaches in the latter category are diverse, with several achieving cubic or sub-cubic scaling. An important technique is transforming to bases where the evaluation of the polarizability is formally cubic scaling. This includes working in real space and imaginary time where the polarizability is separable [23, 24], manipulating the spectral functions in a localized-orbital basis [25], exploiting sparse overlap integrals in a Gaussian basis [26], and using tensor hypercontraction [27] and density-fitting methods [28–30]. Independent of these cubic scaling methods, stochastic approaches [31–34] can achieve linear scaling with system size by working in the time domain. Additionally, there are representations of the theory which still scale quarticly but exhibit lower prefactors, such as within the framework of density-functional perturbation theory [35, 36].

In this letter, we propose a simple and rigorous approach that combines the stochastic and sum-over-bands methods to achieve a quasi-quadratic scaling GW formalism with a small prefactor (speedups of ∼100-fold on systems with tens of atoms), from given input mean-field wavefunctions. It offers large computational savings in both the calculation of the dielectric function and the QP self-energy. The performance gain is achieved by the stochastic compression of all mean-field Kohn-Sham states outside a small energy region around the Fermi level, *including occupied states*.

Our approach is compatible with standard reciprocal-space GW codes and is simple to implement. It is also straightforward to converge independently of the GW code which uses it, and *eliminates sum-over-bands truncation parameters in the GW calculation* by allowing one to include all eigenstates from the mean-field Hamiltonian. These advantages allow the computation of QP properties of complex systems of hundreds of atoms with moderate computational expense, which we demonstrate for several systems. Finally, unlike purely stochastic approaches, we observe speedups with respect to a fully deterministic approach for all system sizes, and not only for large systems. We highlight the applicability of our method on several systems of different dimensionality, including a large-scale problem of a 5.75° twisted bilayer of MoS_2.

Method.—The GW approximation in its most common non-self-consistent form is based on the non-interacting single-particle Green's function,

$$G(\omega) \equiv \sum_{n,\mathbf{k}} \frac{|\phi_{n\mathbf{k}}\rangle \langle \phi_{n\mathbf{k}}|}{\omega - E_{n\mathbf{k}} \mp i\eta} \equiv \sum_{\mathbf{k}} G_{\mathbf{k}}(\omega), \tag{1}$$

where $|\phi_{n\mathbf{k}}\rangle$ are mean-field states, typically obtained from density-functional theory (DFT) calculations, with band index n and wavevector $\mathbf{k}$, $E_{n\mathbf{k}}$ are the corresponding eigenenergies, ω is the evaluation frequency, $\eta = 0^+$, and where the sign is negative (positive) when $E_{n\mathbf{k}}$ is below (above) the Fermi energy. As in other stochastic approaches to GW calculations [31], our method is based on the stochastic resolution of the identity operator, $\lim_{N\to\infty} N^{-1} \sum_{i=1}^{N} |\zeta_i\rangle \langle \zeta_i| = \mathbb{1}$, where off-diagonals vanish with a standard deviation of $1/\sqrt{N}$, and $|\zeta_i\rangle$ are random vectors (see Eq. (5)).

When computing electronic properties within MBPT, it is important to accurately capture the pole structure of G close to the Fermi energy. For instance, the non-interacting polarizability matrix $\chi^0_{\mathbf{G},\mathbf{G}'}(\mathbf{q},\omega)$ at a wavevector $\mathbf{q}$ and planewave indices $\mathbf{G}$ and $\mathbf{G}'$ has poles at frequencies corresponding to the energy difference between conduction (c) and valence

(v) states, $\chi^0_{\mathbf{G},\mathbf{G}'}(\mathbf{q},\omega) \sim \sum_{vc\mathbf{k}} A^{vc}_{\mathbf{G},\mathbf{G}'}(\mathbf{k},\mathbf{q})(\omega \pm (E_{c\mathbf{k}} - E_{v\mathbf{k}}))^{-1}$, where $A^{vc}_{\mathbf{G},\mathbf{G}'}$ are matrix elements. Accurately describing the *low-frequency* behavior of χ^0 is critical in MBPT calculations. This depends sensitively on the pole structure of G close to the Fermi energy, but less so on the pole structure of G at farther frequencies. For instance, when evaluating the electronic self-energy Σ^{GW} within the contour-deformation approach [37–39], Σ^{GW} depends on an integral of the screened Coulomb interaction W along the imaginary frequency axis – for which the pole structure of χ^0 gets smoothed out – plus residues of W are typically evaluated at energies close to the Fermi energy.

This motivates us to express G as one term that contains the exact contributions to the pole structure close to the Fermi energy, $G^P_{\mathbf{k}}$, and another contribution that we write as a sum over N_S subspaces that are farther from the Fermi energy, $G^S_{\mathbf{k}}$,

$$G_{\mathbf{k}}(\omega) \approx G^P_{\mathbf{k}}(\omega) + \sum_S^{N_S} G^S_{\mathbf{k}}(\omega). \tag{2}$$

$G^P_{\mathbf{k}}$ is computed exactly within Eq. 1 for bands $n \in P$, where P is a *small* protected subspace with N_P bands closest to the Fermi energy. This deterministic region contains the states of interest for which QP properties are desired, though it is unnecessary when computing only the polarizability [40]. The remaining subspaces S are still required for accurately expressing the self-energy Σ^{GW}, but their pole structure may be approximated. For each subspace S, we first approximate the near-continuum pole distribution or branch cut at $\{E_{n\mathbf{k}}\}$ for states $n \in S$ with a single pole at an average energy $\bar{E}_{S\mathbf{k}}$. Next, we identify the sum $\sum_{n\in S} |\phi_{n\mathbf{k}}\rangle \langle\phi_{n\mathbf{k}}|$ as a projection onto the subspace S. This projection can be compressed using the stochastic resolution of the identity operator,

$$G^S_{\mathbf{k}}(\omega) \approx \frac{1}{\omega - \bar{E}_{S\mathbf{k}} \mp i\eta} \sum_{i=1}^{N_\xi} |\xi^S_{i,\mathbf{k}}\rangle \langle\xi^S_{i,\mathbf{k}}|\,, \tag{3}$$

where $|\xi^S_{i,\mathbf{k}}\rangle$ are vectors that stochastically project any vector onto the subspace S of interest, and which we denote by *stochastic pseudobands*. Note that the subspaces S can run over both unoccupied and occupied states [see Figure 1(a)].

The number of stochastic pseudobands N_ξ is a convergence parameter and controls the stochastic error of the resolution of the identity. The number of subspaces N_S is also a convergence parameter and controls the error of the average energy approximation. In the limit $N_S, N_\xi \to \infty$, we recover the original Green's function in Eq. (1). The partition Eq. (2) is a *stochastic-deterministic* approach, and allows us to maintain high accuracy for important states close to the Fermi energy while compressing states that are less relevant. Our approach is similar in spirit to other stochastic methods for GW calculations [32–34], but does not require propagation in real-time.

Next, we show how to partition the subspaces $\{S\}$ in Eq. (2) and construct each stochastic pseudoband $|\xi^S_{i,\mathbf{k}}\rangle$. A practical approach is to enforce that the error from each subspace to the Green's function or static polarizability matrix $\chi^0_{\mathbf{G},\mathbf{G}'}(\mathbf{q},\omega = 0)$ is roughly constant. This is achieved by enforcing a constant ratio

$$\mathcal{F} \equiv \frac{\Delta E_S}{\bar{E}_S} = \text{const}, \tag{4}$$

where $\bar{E}_S$ is the average energy of the Kohn-Sham states in each subspace S (referenced to the Fermi level) and ΔE_S is the energy range spanned by S [41]. The ratio $\mathcal{F}$ is inversely proportional to the number of subspaces, $\mathcal{F} \sim 1/N_S$.

Finally, for each subspace S, we construct stochastic pseudobands by taking random linear combinations of Kohn-Sham states in S,

$$|\xi^S_{i,\mathbf{k}}\rangle = \frac{1}{\sqrt{N_\xi}} \sum_{n\in S} \alpha^S_{i,n\mathbf{k}} |\phi_{n\mathbf{k}}\rangle\,, \tag{5}$$

with random phases $\alpha = e^{2\pi i\theta}$ for random $\theta \in [0,1)$, and $i \in \{1,\ldots,N_\xi\}$ are the different stochastic pseudobands that realize the projection onto S.

The proposed stochastic compression can be easily implemented in most MBPT codes that use a spectral representation of G, and we have implemented our developmental version in the BerkeleyGW code [42]. One only needs to modify the input Kohn-Sham orbitals and combine them according to Eq. (5). In particular, no modification of the GW code is required: the pseudobands approach is a pre-processing step to the GW calculation. We also provide a pseudocode [43] and reference implementation [44]. The method as described here focuses on compressing the Green's function for the efficient evaluation of the static dielectric function, which is the quantity of interest in calculations that use plasmon-pole models. Still, a simple extension, whereby one takes ΔE_S to be a constant (ΔE) instead of a quantity proportional to $\bar{E}_S$, allows the evaluation of the inverse dielectric function at arbitrary frequencies with small statistical errors and large computational savings [45]. We stress that our approach is amenable to compressing both valence and conduction states, offering especially large speedups for the computation of the dielectric function, which scales with their product. We summarize the quantities introduced in Table I below.

TABLE I. Pseudobands parameters: 'conv.', 'auto.', and 'aux.' are convergence, automatically determined, and auxiliary parameters, respectively. N_P should be 0 when evaluating the polarizability for large systems and finite to evaluate the GW self-energy of deterministic states.

Parameter	Description	Typical Value
$\mathcal{F}$– conv.	Constant energy ratio Eq. (4)	1% – 2%
N_S– auto.	Number of stochastic subspaces, $N_S \propto\!\!\sim \frac{1}{\mathcal{F}}$	10 – 200
N_ξ– conv.	Number of pseudobands per subspace	2 – 3
N_P– aux.	Number of protected bands	$\geq$0

We note that (1) convergence testing with respect to pseudobands parameters is rarely required, as the typical values listed in Table I were sufficient to converge all systems studied and (2) N_P only needs to be large enough to include

the states of interest for computing the electronic self-energy, and can be zero for computing only the dielectric matrix for both semiconductors and metals [40]. Additionally, our approach *removes the band truncation parameters* employed in the sum-over-states in traditional GW calculations. This is because, when constructing the stochastic pseudobands, we can easily consider all bands from the mean-field Hamiltonian by diagonalizing it with scalable linear algebra packages such as ELPA [46]. While one can benefit from similar speedups from our pseudobands approach when generating input Kohn-Sham states with iterative solvers, directly diagonalizing the DFT Hamiltonian is typically faster and more numerically stable [47].

Results.—We benchmark our stochastic pseudobands approach on systems spanning dimensionality, electronic structure, and screening environment to numerically verify its convergence behavior. We demonstrate quasi-quadratic scaling for GW calculations on ZnO supercells up to 256 atoms while maintaining constant error. Finally, we perform a large-scale calculation of the GW QP bandstructure of a 5.75° twisted MoS_2 moiré bilayer to address questions regarding the emergent electronic structure in twisted 2D materials. Computational details are provided in the Supplemental Material [45]. Specific pseudobands convergence parameters are listed with the computations below (v/c superscripts indicate pseudobands parameters used for valence/conduction states, respectively). Regardless of the system, we note that $N_\xi \geq 2$ should be used, as $N_\xi = 1$ does not resolve the projection over each subspace. Additionally, as currently implemented, compressing *valence* states with stochastic pseudobands does not offer advantages for calculating the self-energy operator (as opposed to the dielectric matrix). This is because the bare exchange contribution to the self-energy Σ^X, which involves matrix elements with occupied states, is very sensitive to the character of the valence wavefunctions. Since the calculation of the self-energy only scales with the *sum* of the valence and conduction bands, compressing valence states does not provide significant acceleration for Σ^{GW} in any case. However, stochastic pseudobands always provide speedups when compressing the conduction states for the operators studied here.

Convergence Behavior.—We show systematic convergence of QP energies for two systems, an isolated benzene molecule and bulk wurtzite ZnO. Additional benchmarks on bilayer MoS_2 and a metallic $Ag_{54}Pd$ nanoparticle are presented in the Supplemental Material [48]. Figure 1 summarizes our approach by comparing the error in QP energies for an isolated benzene molecule and for wurtzite ZnO with respect to the number of bands N_b included in the MBPT calculations – both in the summations to evaluate the dielectric matrix and self-energy. For each value of N_b, we include either the lowest N_b Kohn-Sham orbitals, in the deterministic case, or both a set of N_P Kohn-Sham states in the protected region plus $N_S N_\xi$ stochastic pseudobands, such that $N_b = N_P + N_S N_\xi$. Hence, our tests assess whether, for a fixed computational effort, stochastic pseudobands yields more accurate QP energies by approximating the high-energy

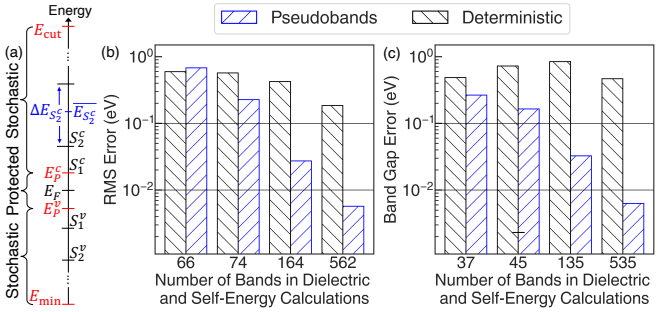

FIG. 1. (a) Diagram of the method's band-partitioning scheme. E_{min} is the energy of the deepest valence state. (b/c) Comparison of the error in the QP energies for GW calculations performed with a traditional deterministic approach and using stochastic pseudobands for (b) an isolated benzene molecule and (c) bulk wurtzite ZnO. Stochastic pseudobands reach converged QP energies (within 10-100 meV) with fewer total bands than a deterministic truncation of the Hilbert space. Pseudobands parameters are (b) $N_P^c = 50$ and (c) $N_P^c = 10$; both (b) and (c) used $N_\xi^c = 2$ and $N_S^c = \{1, 5, 50, 250\}$ (corresponding to $\mathcal{F}^c = \{1.9, 0.42, 0.054, 0.015\}$). Pseudobands were not used to compress valence states.

part of the Hilbert space that gets truncated in deterministic calculations. Figure 1(b) shows the root mean square (RMS) error $\sqrt{\frac{1}{N}\sum_n^N \left(E_n^{\text{QP}} - E_n^{\text{ref}}\right)^2}$ over 19 QP levels around the Fermi energy of benzene for both the deterministic calculation and pseudobands. Figure 1(c) shows the error of the bandgap $\left|E_{\text{gap}}^{\text{QP}} - E_{\text{gap}}^{\text{ref}}\right|$ of ZnO, again comparing both the deterministic calculations and those using stochastic pseudobands. In both cases, E^{ref} is obtained from a highly converged deterministic calculation – utilizing 30,000 bands for benzene and 10,000 bands for ZnO.

For both materials, stochastic pseudobands outperforms the deterministic results by 10-100-fold in error for the same computational effort for all but the least converged calculations. Conversely, we find that, to achieve the same error, the deterministic calculation requires approximately 10-100 times as many bands as used in stochastic pseudobands calculations. We see rapid and systematic convergence behavior for all systems studied.

Scaling and Computational Cost.—In addition to the good convergence behavior, utilization of stochastic pseudobands also significantly improves the computational scaling of the GW approach with system size. Traditionally, the calculation of the dielectric matrix consists of two primary computationally demanding steps: constructing the non-interacting polarizability matrix $\chi^0_{\mathbf{G},\mathbf{G}'}$, which scales as $\mathcal{O}(N_{\mathbf{G}}^2 \times N_c \times N_v) \sim \mathcal{O}(N^4)$, and then inverting the RPA dielectric matrix $\epsilon_{\mathbf{G},\mathbf{G}'}$, which scales as $\mathcal{O}(N_{\mathbf{G}}^3) \sim \mathcal{O}(N^3)$, where N_v and N_c are the numbers of valence and conduction bands, and $N_{\mathbf{G}}$ and N are the number of reciprocal-lattice vectors and the overall system size, respectively. With stochastic pseudobands, the cost to compute the noninteracting polarizability is $\mathcal{O}(N_G^2 N_S^2 N_\xi^2)$, since one can always take $N_P = 0$. It still takes $\mathcal{O}(N^3)$ to in-

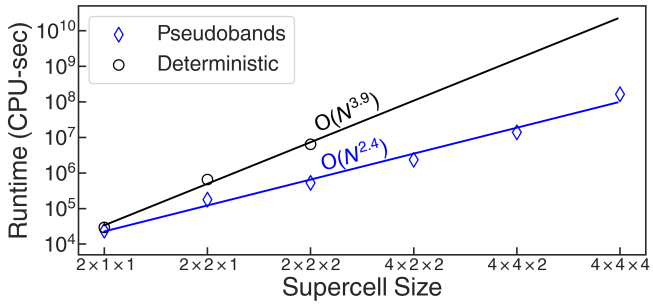

FIG. 2. Scaling curve for the dielectric computation per q/k-point for ZnO supercells showing quasi-quadratic behavior up to 256 atoms. Bandgap errors are maintained at < 50 meV for constant convergence parameters $N_\xi, \mathcal{F}$ [48].

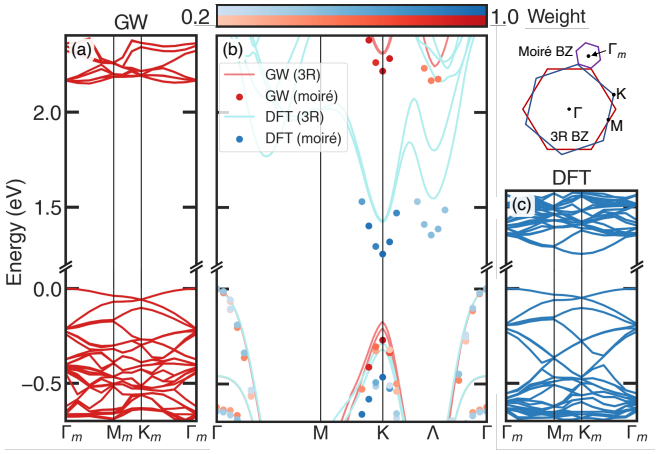

FIG. 3. (a/c) GW (computed with stochastic pseudobands) and DFT band structure for the 5.75°-twisted moiré system in the moiré BZ. (b) Band structure for the untwisted, 3R-stacked MoS_2 bilayer (solid lines) and the corresponding unfolded band structure of the 5.75° twisted moiré system (dots), at the DFT and GW levels. The weight of the projection represents the contribution of the unit cell state to the corresponding moiré state at the same energy. Inset above (c): BZs of the twisted and untwisted structures.

vert the dielectric matrix, although that cost can be reduced with low-rank techniques [49–51], making the GW workflow quasi-quadratic. Our results show that the computational savings are insensitive to the details of N_P (see Figure 2). Additionally, from Eq. (4), the total number of states when utilizing pseudobands is roughly the logarithm of the initial number of states, yielding a significant reduction in the number of states used in the MBPT calculations and a low algorithmic prefactor. Moreover, due to the high performance of distributed-memory linear algebra solvers, we find that the inversion of the dielectric matrix is only a significant bottleneck for large systems, with hundreds to thousands of atoms in the unit cell. In fact, for the largest system we studied of 5.75° twisted bilayer MoS_2, inversion took only 14% of the total run time.

Figure 2 shows the computational scaling for calculating a well-converged dielectric matrix for ZnO, with a plane-wave cutoff of 80 Ry, where we consider systematically larger supercells containing from 8 to 256 atoms [45]. To make these calculations feasible, it was critical to use our approach wherein both valence and conduction states away from the Fermi energy are compressed into stochastic pseudobands. All supercells exhibited constant error < 50 meV when we performed subsequent self-energy calculations of the quasiparticle energies with unchanged convergence parameters ($N_\xi^v = 4$, $N_\xi^c = 2$, $\mathcal{F}^{v/c} = 0.02$). $N_P^{v/c}$ was chosen to be 20 for the $2 \times 1 \times 1$ supercell and scales with the system size to allow for the evaluation of the self-energy within the same energy window [40, 45, 48]). Even with a nonzero N_P, we find that the approach displays in practice a *quasi-quadratic scaling* for the evaluation of the dielectric function and self-energy.

Application to Large Systems.— Moiré bilayers such as twisted bilayer graphene or transition metal dichalcogenides (TMDs) have been at the research forefront for investigating correlated electronic phases in condensed matter systems [10, 52–56]. Semiconducting TMD moiré bilayers have gained additional interest as hosts of different types of emergent excitons for possible applications in optoelectronic and exciton-based qubit devices [57–67]. A correct description of the QP properties is often a prerequisite to understanding these emergent phenomena, but the large system size and variations of the dielectric function [68, 69] requiring fine Brillouin zone (BZ) samplings [70] has made them difficult to study with first-principles GW calculations.

Using the pseudobands approach, we perform explicit GW calculations on a 5.75°-twisted bilayer of MoS_2 containing 546 atoms in the moiré supercell [Figure 3(a)], and further unfold the moiré band structure to the unit cell of the high-symmetry, 0°-twisted bilayer structure [71, 72], known as the 3R stacking [red dots in Figure 3(b)]. We compare such large-scale GW calculations to DFT calculations performed directly on the 3R structure [blue lines in Figure 3(b)] and find differences in the bandgap, the relative energy splitting, and band ordering.

We rationalize these differences through contributions from moiré and quasiparticle effects. To understand moiré effects, we perform DFT calculations on the twisted structure [Figure 3(c)] and unfold the resulting band structure onto the BZ of the 3R structure [blue dots in Figure 3(b)]. Compared to direct DFT calculations on the 3R structure, the DFT calculations on the 5.75°-twisted system display a larger energy splitting between the first two valence states at Γ. This is expected since these states originate from the interlayer chalcogen interactions, which change with stacking and twist angle. Next, to capture quasiparticle effects, we perform GW calculations on the 3R structure [red lines in Figure 3(b)]. Compared again to the DFT calculation on the 3R structure, QP effects mainly increase the bandgap and reorder the conduction states at the K and Λ valleys. Our calculations highlight that moiré effects and quasiparticle corrections both play significant roles in twisted materials and need to be accounted for on the same

footing [17], and are additive here to within 100 meV [73].

Conclusion.—We present a mixed stochastic-deterministic approach for GW calculations. Given input mean-field states, the method displays quasi-quadratic scaling for the tests performed up to 256 atoms, ∼100-fold speedups for systems of tens of atoms, and smooth convergence behavior. The usage of stochastic pseudobands is compatible with systems of any dimension, nontrivial screening environments, and extends standard MBPT codes to handle systems of several hundreds of atoms with moderate computational expense. We envision that, beyond further studies on moiré systems, structurally large and technologically relevant systems such as interfaces, surfaces, and extended defects can be studied with this approach to address fundamental questions involving the interplay between nonlocal screening environments and self-energy effects.

ARA acknowledges helpful discussions with Mauro Del Ben, Johnathan D. Georgaras, and Emma M. Simmerman. This work was primarily supported by the Center for Computational Study of Excited-State Phenomena in Energy Materials (C2SEPEM), funded by the U.S. Department of Energy (DOE), Office of Basic Energy Sciences (BES) under Contract No. DE-AC02-05CH11231 at the Lawrence Berkeley National Laboratory (LBL), as part of the Computational Materials Sciences Program. The study of twisted MoS_2 was supported by the U.S. DOE BES grant DE-SC0021984. This research used resources of the National Energy Research Scientific Computing Center (NERSC), a U.S. DOE Office of Science User Facility located at LBL, operated under Contract No. DE-AC02-05CH11231 using NERSC award BES-ERCAP m3606, and from the Texas Advanced Computing Center (TACC) at The University of Texas at Austin, funded by the National Science Foundation (NSF) award 1818253, through allocation DMR21077 for the development of algorithms. Large-scale calculations used resources of the Oak Ridge Leadership Computing Facility at the Oak Ridge National Laboratory, which is supported by the U.S. DOE BES under Contract No. DE-AC05-00OR22725.

† jornada@stanford.edu

[1] L. Hedin and S. Lundqvist, in *Solid state physics*, Vol. 23 (Elsevier, 1970) pp. 1–181.
[2] M. S. Hybertsen and S. G. Louie, Physical Review B **34**, 5390 (1986).
[3] G. Onida, L. Reining, and A. Rubio, Reviews of modern physics **74**, 601 (2002).
[4] M. L. Cohen and S. G. Louie, *Fundamentals of condensed matter physics* (Cambridge University Press, 2016).
[5] S. G. Louie and M. L. Cohen, *Conceptual foundations of materials: a standard model for ground-and excited-state properties* (Elsevier, 2006).
[6] B. Sahni, Vikram, J. Kangsabanik, and A. Alam, The Journal of Physical Chemistry Letters **11**, 6364 (2020).
[7] M. Van Setten, M. Giantomassi, X. Gonze, G.-M. Rignanese, and G. Hautier, Physical Review B **96**, 155207 (2017).
[8] M. J. van Setten, F. Caruso, S. Sharifzadeh, X. Ren, M. Scheffler, F. Liu, J. Lischner, L. Lin, J. R. Deslippe, S. G. Louie, *et al.*, Journal of chemical theory and computation **11**, 5665 (2015).
[9] A. Stuke, C. Kunkel, D. Golze, M. Todorović, J. T. Margraf, K. Reuter, P. Rinke, and H. Oberhofer, Scientific data **7**, 58 (2020).
[10] D. M. Kennes, M. Claassen, L. Xian, A. Georges, A. J. Millis, J. Hone, C. R. Dean, D. N. Basov, A. N. Pasupathy, and A. Rubio, Nature Physics **17**, 155 (2021).
[11] M. H. Naik, S. Kundu, I. Maity, and M. Jain, Phys. Rev. B **102**, 075413 (2020).
[12] F. Wu, T. Lovorn, E. Tutuc, I. Martin, and A. H. MacDonald, Phys. Rev. Lett. **122**, 086402 (2019).
[13] M. Angeli and A. H. MacDonald, Proceedings of the National Academy of Sciences **118**, e2021826118 (2021).
[14] S. Carr, S. Fang, and E. Kaxiras, Nature Reviews Materials **5**, 748 (2020).
[15] K. Tran, J. Choi, and A. Singh, 2D Materials **8**, 022002 (2020).
[16] L. Xian, M. Claassen, D. Kiese, M. M. Scherer, S. Trebst, D. M. Kennes, and A. Rubio, Nature communications **12**, 5644 (2021).
[17] X. Lu, X. Li, and L. Yang, Physical Review B **100**, 155416 (2019).
[18] G. Samsonidze, M. Jain, J. Deslippe, M. L. Cohen, and S. G. Louie, Physical Review Letters **107**, 186404 (2011).
[19] W. Gao, W. Xia, X. Gao, and P. Zhang, Scientific reports **6**, 36849 (2016).
[20] F. Bruneval and X. Gonze, Physical Review B **78**, 085125 (2008).
[21] J. Deslippe, G. Samsonidze, M. Jain, M. L. Cohen, and S. G. Louie, Physical Review B **87**, 165124 (2013).
[22] J. Berger, L. Reining, and F. Sottile, Physical Review B **82**, 041103 (2010).
[23] P. Liu, M. Kaltak, J. Klimeš, and G. Kresse, Physical Review B **94**, 165109 (2016).
[24] M. Kim, G. J. Martyna, and S. Ismail-Beigi, Physical Review B **101**, 035139 (2020).
[25] D. Foerster, P. Koval, and D. Sánchez-Portal, The Journal of chemical physics **135**, 074105 (2011).
[26] J. Wilhelm, D. Golze, L. Talirz, J. Hutter, and C. A. Pignedoli, The journal of physical chemistry letters **9**, 306 (2018).
[27] R. M. Parrish, E. G. Hohenstein, N. F. Schunck, C. D. Sherrill, and T. J. Martínez, Physical Review Letters **111**, 132505 (2013).
[28] A. Förster and L. Visscher, Journal of chemical theory and computation **16**, 7381 (2020).
[29] H. Ma, L. Wang, L. Wan, J. Li, X. Qin, J. Liu, W. Hu, L. Lin, C. Yang, and J. Yang, The Journal of Physical Chemistry A **125**, 7545 (2021).
[30] I. Duchemin and X. Blase, Journal of Chemical Theory and Computation **17**, 2383 (2021).
[31] D. Neuhauser, Y. Gao, C. Arntsen, C. Karshenas, E. Rabani, and R. Baer, Physical review letters **113**, 076402 (2014).
[32] V. Vlček, E. Rabani, D. Neuhauser, and R. Baer, Journal of chemical theory and computation **13**, 4997 (2017).
[33] V. Vlček, W. Li, R. Baer, E. Rabani, and D. Neuhauser, Physical Review B **98**, 075107 (2018).
[34] M. Romanova and V. Vlček, npj Computational Materials **8**, 11 (2022).
[35] F. Giustino, M. L. Cohen, and S. G. Louie, Physical Review B **81**, 115105 (2010).
[36] M. Govoni and G. Galli, Journal of chemical theory and computation **11**, 2680 (2015).
[37] A. Oschlies, R. Godby, and R. Needs, Physical Review B **51**,

1527 (1995).
[38] S. Lebègue, B. Arnaud, M. Alouani, and P. Bloechl, Physical Review B **67**, 155208 (2003).
[39] F. Bruneval, PhD Thesis (2005).
[40] See Supplemental Material, section S3.2.2, at XXX for discussion about the value of N_P.
[41] See Supplemental Material, section S3, at XXX for further information about convergence derivations, which includes Refs. [2, 34, 37–39, 74].
[42] J. Deslippe, G. Samsonidze, D. A. Strubbe, M. Jain, M. L. Cohen, and S. G. Louie, Computer Physics Communications **183**, 1269 (2012).
[43] See Supplemental Material, section S1.6, at XXX for a pseudocode implementation of the pseudobands approach.
[44] A. R. Altman, S. Kundu, and F. H. da Jornada, "Supplemental Datasets for Manuscript: Mixed Stochastic-Deterministic Approach for Many-Body Perturbation Theory Calculations," (2023).
[45] See Supplemental Material, section S1, at XXX for computational details, which includes Refs. [2, 8, 42, 51, 75–87].
[46] A. Marek, V. Blum, R. Johanni, V. Havu, B. Lang, T. Auckenthaler, A. Heinecke, H.-J. Bungartz, and H. Lederer, Journal of Physics: Condensed Matter **26**, 213201 (2014).
[47] See Supplemental Material, section S1.5, at XXX for further information about direct diagonalization of the mean-field Hamiltonian, which includes Ref. [46].
[48] See Supplemental Material section S2 at XXX for additional convergence tests.
[49] H. F. Wilson, F. Gygi, and G. Galli, Physical Review B **78**, 113303 (2008).
[50] M. Shao, L. Lin, C. Yang, F. Liu, F. H. Da Jornada, J. Deslippe, and S. G. Louie, Science China Mathematics **59**, 1593 (2016).
[51] M. Del Ben, F. H. da Jornada, G. Antonius, T. Rangel, S. G. Louie, J. Deslippe, and A. Canning, Physical Review B **99**, 125128 (2019).
[52] E. Y. Andrei, D. K. Efetov, P. Jarillo-Herrero, A. H. MacDonald, K. F. Mak, T. Senthil, E. Tutuc, A. Yazdani, and A. F. Young, Nature Reviews Materials **6**, 201 (2021).
[53] Z. Zheng, Q. Ma, Z. Bi, S. de La Barrera, M.-H. Liu, N. Mao, Y. Zhang, N. Kiper, K. Watanabe, T. Taniguchi, *et al.*, Nature **588**, 71 (2020).
[54] Y. Cao, V. Fatemi, S. Fang, K. Watanabe, T. Taniguchi, E. Kaxiras, and P. Jarillo-Herrero, Nature **556**, 43 (2018).
[55] L. Wang, E.-M. Shih, A. Ghiotto, L. Xian, D. A. Rhodes, C. Tan, M. Claassen, D. M. Kennes, Y. Bai, B. Kim, K. Watanabe, T. Taniguchi, X. Zhu, J. Hone, A. Rubio, A. N. Pasupathy, and C. R. Dean, Nature Materials **19**, 861 (2020).
[56] Y. Xu, S. Liu, D. A. Rhodes, K. Watanabe, T. Taniguchi, J. Hone, V. Elser, K. F. Mak, and J. Shan, Nature **587**, 214 (2020).
[57] K. Tran, G. Moody, F. Wu, X. Lu, J. Choi, K. Kim, A. Rai, D. A. Sanchez, J. Quan, A. Singh, *et al.*, Nature **567**, 71 (2019).
[58] H. Yu, G.-B. Liu, J. Tang, X. Xu, and W. Yao, Science advances **3**, e1701696 (2017).
[59] T. I. Andersen, G. Scuri, A. Sushko, K. De Greve, J. Sung, Y. Zhou, D. S. Wild, R. J. Gelly, H. Heo, D. Bérubé, A. Y. Joe, L. A. Jauregui, K. Watanabe, T. Taniguchi, P. Kim, H. Park, and M. D. Lukin, Nature Materials **20**, 480 (2021).
[60] M. H. Naik, E. C. Regan, Z. Zhang, Y.-H. Chan, Z. Li, D. Wang, Y. Yoon, C. S. Ong, W. Zhao, S. Zhao, M. I. B. Utama, B. Gao, X. Wei, M. Sayyad, K. Yumigeta, K. Watanabe, T. Taniguchi, S. Tongay, F. H. da Jornada, F. Wang, and S. G. Louie, Nature **609**, 52 (2022).
[61] L. A. Jauregui, A. Y. Joe, K. Pistunova, D. S. Wild, A. A. High, Y. Zhou, G. Scuri, K. De Greve, A. Sushko, C.-H. Yu, *et al.*, Science **366**, 870 (2019).
[62] O. Karni, E. Barré, S. C. Lau, R. Gillen, E. Y. Ma, B. Kim, K. Watanabe, T. Taniguchi, J. Maultzsch, K. Barmak, R. H. Page, and T. F. Heinz, Phys. Rev. Lett. **123**, 247402 (2019).
[63] O. Karni, E. Barré, V. Pareek, J. D. Georgaras, M. K. L. Man, C. Sahoo, D. R. Bacon, X. Zhu, H. B. Ribeiro, A. L. O'Beirne, J. Hu, A. Al-Mahboob, M. M. M. Abdelrasoul, N. S. Chan, A. Karmakar, A. J. Winchester, B. Kim, K. Watanabe, T. Taniguchi, K. Barmak, J. Madéo, F. H. da Jornada, T. F. Heinz, and K. M. Dani, Nature **603**, 247 (2022).
[64] Y. Tang, J. Gu, S. Liu, K. Watanabe, T. Taniguchi, J. Hone, K. F. Mak, and J. Shan, Nature Nanotechnology **16**, 52 (2021).
[65] K. L. Seyler, P. Rivera, H. Yu, N. P. Wilson, E. L. Ray, D. G. Mandrus, J. Yan, W. Yao, and X. Xu, Nature **567**, 66 (2019).
[66] Y. Shimazaki, I. Schwartz, K. Watanabe, T. Taniguchi, M. Kroner, and A. Imamoğlu, Nature **580**, 472 (2020).
[67] C. Jin, J. Kim, M. I. B. Utama, E. C. Regan, H. Kleemann, H. Cai, Y. Shen, M. J. Shinner, A. Sengupta, K. Watanabe, *et al.*, Science **360**, 893 (2018).
[68] S. Latini, T. Olsen, and K. S. Thygesen, Physical Review B **92** (2015).
[69] D. Y. Qiu, F. H. da Jornada, and S. G. Louie, Physical Review B **93** (2016).
[70] F. H. da Jornada, D. Y. Qiu, and S. G. Louie, Physical Review B **95** (2017).
[71] S. Kundu, T. Amit, H. R. Krishnamurthy, M. Jain, and S. Refaely-Abramson, npj Computational Materials **9**, 186 (2023).
[72] V. Popescu and A. Zunger, Physical Review B **85**, 085201 (2012).
[73] See Supplemental Material, section S2.2.1, at XXX for discussion on extrapolation of GW corrections from unit cells to moiré cells.
[74] R. Baer, D. Neuhauser, and E. Rabani, Physical review letters **111**, 106402 (2013).
[75] P. Giannozzi, S. Baroni, N. Bonini, M. Calandra, R. Car, C. Cavazzoni, D. Ceresoli, G. L. Chiarotti, M. Cococcioni, I. Dabo, *et al.*, Journal of physics: Condensed matter **21**, 395502 (2009).
[76] J. P. Perdew, K. Burke, and M. Ernzerhof, Physical review letters **77**, 3865 (1996).
[77] M. J. van Setten, M. Giantomassi, E. Bousquet, M. J. Verstraete, D. R. Hamann, X. Gonze, and G.-M. Rignanese, Computer Physics Communications **226**, 39 (2018).
[78] M. Schlipf and F. Gygi, Computer Physics Communications **196**, 36 (2015).
[79] S. Ismail-Beigi, Physical Review B **73**, 233103 (2006).
[80] R. T. Downs and M. Hall-Wallace, American Mineralogist **88**, 247 (2003).
[81] T. Rangel, M. Del Ben, D. Varsano, G. Antonius, F. Bruneval, F. H. da Jornada, M. J. van Setten, O. K. Orhan, D. D. O'Regan, A. Canning, *et al.*, Computer Physics Communications **255**, 107242 (2020).
[82] A. H. Larsen, J. J. Mortensen, J. Blomqvist, I. E. Castelli, R. Christensen, M. Dułak, J. Friis, M. N. Groves, B. Hammer, C. Hargus, *et al.*, Journal of Physics: Condensed Matter **29**, 273002 (2017).
[83] A. P. Thompson, H. M. Aktulga, R. Berger, D. S. Bolintineanu, W. M. Brown, P. S. Crozier, P. J. in't Veld, A. Kohlmeyer, S. G. Moore, T. D. Nguyen, *et al.*, Computer Physics Communications **271**, 108171 (2022).
[84] M. H. Naik, I. Maity, P. K. Maiti, and M. Jain, The Journal of Physical Chemistry C **123**, 9770 (2019).

[85] J.-W. Jiang, H. S. Park, and T. Rabczuk, Journal of Applied Physics **114**, 064307 (2013).
[86] F. H. da Jornada, D. Y. Qiu, and S. G. Louie, Physical Review B **95**, 035109 (2017).
[87] D. Y. Qiu, F. H. da Jornada, and S. G. Louie, Physical review letters **111**, 216805 (2013).